Two-dimensional alloy of immiscible metals: Single and binary monolayer films of Pb and Sn on Rh(111)

J. Yuhara,[1,2,*] M. Schmid,[2] and P. Varga[2]
[1]*Department of Crystalline Materials Science, School of Engineering, Nagoya University, Furo-cho, Chikusa-ku, Nagoya 464-8603, Japan*
[2]*Institut für Allgemeine Physik, Technische Universität Wien, Wiedner Hauptstraße 8-10, A-1040 Wien, Austria*
(Received 23 January 2003; published 12 May 2003)

The single and binary metal films of Pb and Sn on Rh(111) have been studied at room temperature by scanning tunneling microscopy (STM), low-energy electron diffraction, and Auger electron spectroscopy. Both Pb and Sn are mobile at low coverage and form commensurate overlayers of (4×4)-Pb and $c(2\times4)$-Sn, respectively. From atomically resolved STM images, the atomic arrangements of (4×4)-Pb and $c(2\times4)$-Sn have been identified to be hexagonal and rectangular structures, respectively. With increasing coverage, both commensurate phases change into incommensurate phases followed by island formation (Stranski-Krastanov growth). This shows that Rh(111) is static and inert enough to support two-dimensional (2D) phases of Pb and/or Sn without alloying at room temperature. The Pb-Sn bimetallic film on Rh(111) forms an ordered 2D alloy of $PbSn_3$ with an incommensurate structure close to $(\sqrt{7}\times\sqrt{7})$, contrary to the immiscibility of Pb and Sn in the bulk. From atomically resolved STM images, the atomic arrangement of this $(\sqrt{7}\times\sqrt{7})$-(Pb,Sn) structure has been determined.

DOI: 10.1103/PhysRevB.67.195407 PACS number(s): 68.55.Jk, 68.37.Ef, 68.43.Fg, 68.55.Nq

I. INTRODUCTION

The formation processes and mechanisms of heteroepitaxial metal-on-metal growth have been studied intensively because of their importance not only for fundamental aspects but also industrial applications like coatings, catalysis, etc.[1,2] Many of the systems form monolayer surface alloys of the substrate and deposited material, even though they are immiscible in bulk.[3–7] Recently, bimetallic films of the immiscible metals Pb and Sn on the Si(111) surface were found to form PbSn, $PbSn_2$, and Pb_2Sn surface alloys with so-called $(\sqrt{7}\times\sqrt{3})$, $(2\sqrt{7}\times3)$, and $(\sqrt{3}\times\sqrt{3})$ structures.[8–11] Since the Pb and/or Sn films lead to a restructuring of the Si(111) surface and form only commensurate phases there, the Si substrate may play an important role for the stabilization of Pb-Sn surface alloys. To understand the mechanism and the difference between two-dimensional (2D) surface phases and three-dimensional (3D) bulk phases, it is necessary to study the purely 2D bimetallic film using a more static and inert substrate.

In the present paper, we show the 2D system of Pb-Sn monolayer films on Rh(111), which is found to be an ideal substrate to examine the lateral atomic interaction of Pb and Sn. In this system, we found strong evidence for the 2D-ordered alloy of $PbSn_3$ using atomically resolved scanning tunneling microscopy (STM).

II. EXPERIMENT

The STM experiments were performed in an ultrahigh-vacuum chamber equipped with a customized Omicron room-temperature micro-STM, low-energy electron diffraction (LEED) optics, an Auger electron spectrometer with a cylindrical mirror analyzer, and a mass spectrometer for residual gas analysis. The base pressure of the chamber is below 1.0×10^{-10} mbar. All STM images were obtained in constant current mode with the sample negative. The sample was prepared in a separate UHV chamber with a base pressure below 1.0×10^{-10} mbar. The Rh(111) surface was cleaned by cycles of 2 keV Ar^+ sputtering at room temperature (RT) followed by annealing at 1150 K. The cleanliness of the Rh(111) surface was checked by Auger electron spectroscopy (AES); no contaminations such as C and O could be observed within the detection limits. The clean Rh(111) surface exhibited a distinct (1×1) LEED pattern. The size of the terraces of the sample was found to be 10–50 nm from STM images. Sn and/or Pb were deposited onto the Rh(111) surface at room temperature using electron-beam-heated Mo crucibles in a water-cooled evaporator at deposition rates of about 1 monolayer/min, measured by a quartz crystal microbalance. A retarding voltage was applied to the end of the evaporator in order to suppress high-energy Sn and Pb ions from the evaporators, since such ions create atomic defects at the sample surface.[5] The error in Sn and Pb coverage was estimated from repeated measurements to be less than 5% as determined from the Auger peak-to-peak signal ratios of Sn(430 eV)/Rh(302 eV) and Pb(94 eV)/Rh(302 eV). We define one monolayer (ML) as an overlayer with the atomic density of a Rh(111) layer.

III. RESULTS

This section is separated into three subsections. In the first two subsections, we present the results from single metal films of Sn and Pb on Rh(111). In the last subsection, the results from a Pb-Sn bimetallic film on Rh(111) are presented.

A. Sn films on Rh(111)

Figure 1 shows typical LEED patterns of Sn films at 0.45 ML (a), 0.55 ML (b), and 0.65 ML (c) in thickness deposited

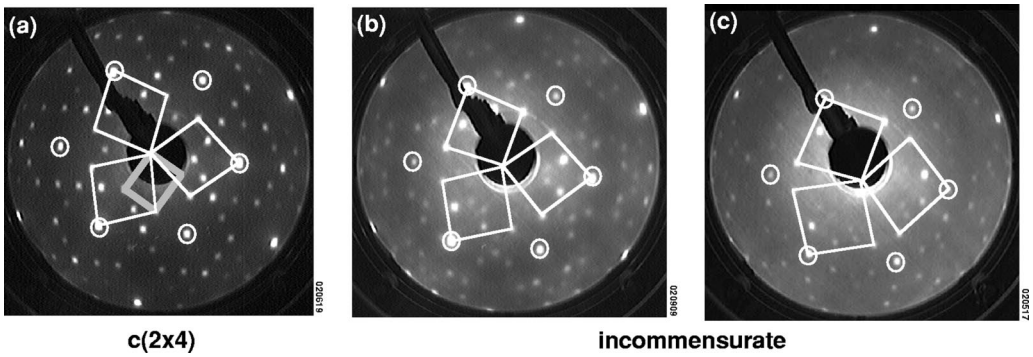

FIG. 1. LEED patterns at 141 eV incident electron energy of Sn/Rh(111) surfaces at coverages of (a) 0.45 ML, (b) 0.55 ML, (c) and 0.65 ML. The first-order Rh(111) substrate spots are marked by open circles. The reciprocal $c(2\times4)$ unit cell is illustrated by the gray rectangle in (a). Three equivalent orientations of the reciprocal rhombic unit cells are also shown.

on Rh(111) at RT. At a Sn coverage below 0.5 ML, a $c(2\times4)$ pattern is clearly observed. The primitive cell of this pattern in real space is rectangular with side lengths of $2a$ (along [110]) and $\sqrt{3}a$. There are three equivalent orientations of the unit cells as illustrated in the figure. At higher coverage, we find an incommensurate (IC) phase similar to the $c(2\times4)$, but with a decreasing lattice real-space lattice constants. The contraction of the IC phase with respect to the $c(2\times4)$ unit cell occurs in the [110] direction, as shown later in Fig. 3(c).

Figure 2 shows STM images of Sn films deposited on Rh(111) at RT. At coverages below 0.5 ML, Sn atoms form 2D islands with frizzy steps [Fig. 2(a)]. This means that Sn atoms are mobile at the edges of the Rh(111)$c(2\times4)$-Sn islands. The area of the Sn islands after deposition of 0.25 ML is estimated to be about 35% [Fig. 2(a)]. If all Sn atoms deposited form islands with the $c(2\times4)$ structure derived from LEED, nearly 50% of the surface would be covered. Therefore, from the relationship between the area of Sn islands and Sn coverage deposited, some Sn atoms must be considered invisible, probably due to their high mobility on the Rh(111) surface. Moreover, in this coverage regime we have observed indications of a strong (repulsive) interaction of the Sn atoms with the tip: if the sample voltage is positive, the STM images show only the Rh(111)(1×1) surface. At coverages above 0.6 ML, 3D Sn islands are formed at the step edges, especially on the upper terrace, as shown in Fig. 2(b). The section profiles at the lines in the STM images in Figs. 2(a) and 2(b) are shown in Figs. 2(c) and 2(d). The $c(2\times4)$-Sn islands appear 0.22 nm higher than Rh(111) clean surface. The Sn 3D islands at higher coverage protrude 0.3–0.5 nm from the first Sn layer, which corresponds to one or two additional Sn layers.

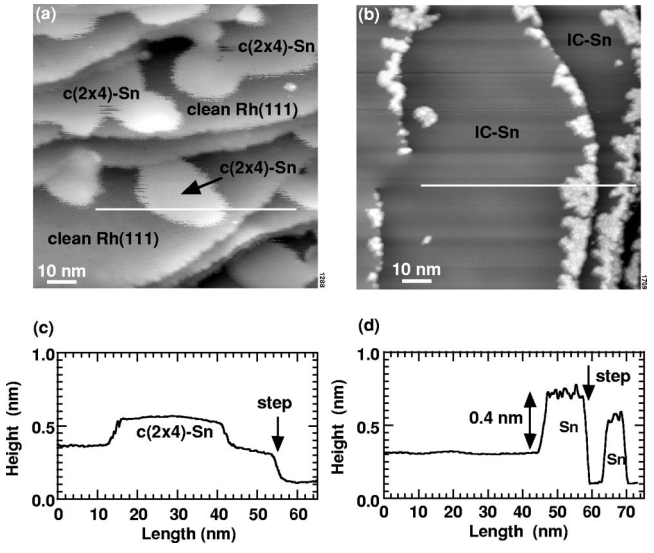

FIG. 2. Large-scale STM images (100×100 nm^2) of Sn/Rh(111) at (a) subsaturation coverage ($\theta_{Sn}=0.25$ ML, $V=-320$ mV, $I=0.46$ nA) and (b) oversaturation coverage ($\theta_{Sn}=0.65$ ML, $V=-9.1$ mV, $I=0.58$ nA). (c) and (d) are section profiles along the white lines in (a) and (b), respectively.

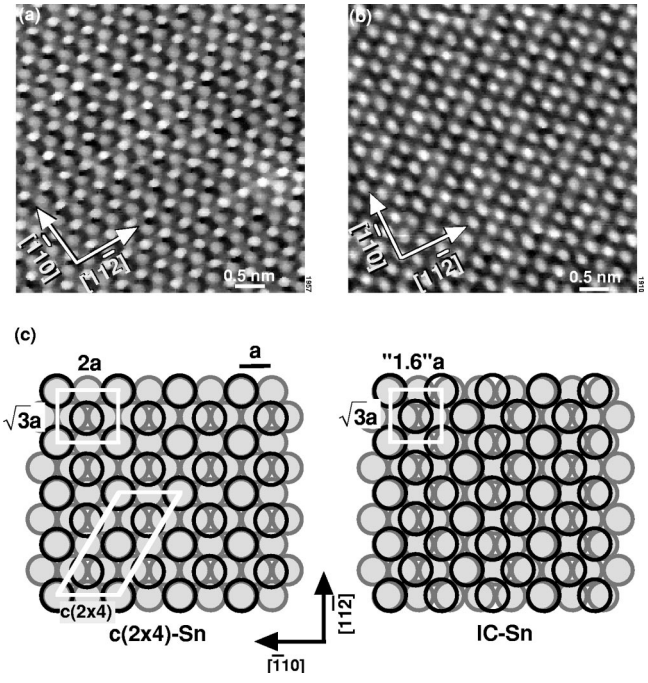

FIG. 3. Atomically resolved STM images (5×5 nm^2) of Sn/Rh(111) at (a) subsaturation coverage ($V=-6.6$ mV, $I=0.46$ nA) and (b) oversaturation coverage ($V=-0.5$ mV, $I=3.4$ nA). (c) Structure model corresponding to these two phases, $c(2\times4)$-Sn and incommensurate (IC) Sn.

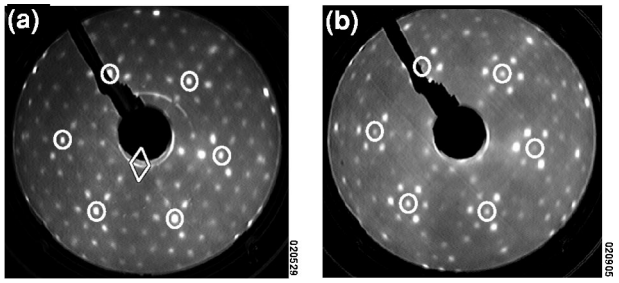

FIG. 4. LEED patterns at 141 eV incident electron energy of Pb/Rh(111) surfaces at coverages of (a) 0.5 ML and (b) 1.0 ML. The first-order Rh(111) substrate spots are marked by open circles. The reciprocal (4×4) unit cell is illustrated by the white rhomb in (a).

Figures 3(a) and 3(b) show atomic resolution STM images of the $c(2\times4)$-Sn and IC-Sn structures. We can see two bright spots per primitive rectangular unit cell. On the $c(2\times4)$-Sn surface, these two spots have an ≈10 pm apparent height difference, reflecting two different adsorption sites for Sn on the Rh(111) surface. In contrast to this, the IC-Sn surface shows uniformly bright spots, reflecting no specific adsorption site. There is also no moiré pattern observed. As already indicated by LEED, when the Sn coverage increases from 0.5 ML to 0.6 ML, the surface structure changes from commensurate $c(2\times4)$-Sn into a compressed incommensurate structure, and the Sn atoms are compressed in the [110] direction, as illustrated in Fig. 3(c). However, the registry of the $c(2\times4)$-Sn on the Rh layer below, i.e., whether the Sn atoms occupy top, bridge, or hollow sites, cannot be unambiguously determined from the STM images. Given the two different apparent heights of the Sn atoms in the $c(2\times4)$ structure, we considered a model with top and bridge sites most likely, whereas a structure with the Sn atoms near fcc and hcp hollow sites would probably lead to a smaller height difference. Assuming Sn atoms in top and bridge sites is also in line with the general trend that metal adatoms and overlayers with a lattice constant significantly larger than that of the substrate are strongly bound in on-top sites of close-packed surfaces (see, e.g., Refs. 12–15). The nearest-neighbor distances of Sn atoms are 0.36 nm for $c(2\times4)$-Sn and 0.32–0.34 nm for IC-Sn as determined from LEED and STM images. These values are slightly larger than those for bulk Sn, where the interatomic distances are 0.28 nm and 0.30 nm for α-Sn and β-Sn, respectively.

B. Pb films on Rh(111)

Figure 4 shows typical LEED patterns of Pb films with coverages of (a) 0.5 ML and (b) 1.0 ML deposited on Rh(111) at RT. At Pb coverages of 0.5 ML and below, a (4×4) pattern is observed. At higher coverages, above 0.6 ML, the LEED image shows an incommensurate pattern between (4×4) and (5×5), as shown in Fig. 4 (b). We conclude that the interatomic distance of the Pb atoms at coverages of 0.5 ML and below is approximately 4/3 of the atomic distance of the Rh atoms; i.e., the length required for three Pb atoms matches that of four Rh atoms in the Rh(111) surface.

Figures 5(a) and 5(b) show the corresponding STM images. At Pb coverages of 0.5 ML or below, STM images show only a lattice with an interatomic distance of 0.27 nm [Fig. 5(a), inset], which corresponds to the atomic distance of the Rh atoms (0.269 nm). Nevertheless, as mentioned before, at coverages between 0.3 ML and 0.5 ML the LEED image exhibits a clear (4×4) pattern [Fig. 4(a)]. This indicates that the Pb islands existing on the Rh(111) surface are too mobile to be imaged by STM at room temperature and possibly invisible due to tip-sample interaction, similar to Sn at positive voltage. At Pb coverages above 0.6 ML, the first Pb monolayer is visible in the STM images and three-dimensional Pb islands grow along the step [Fig. 5(b), inset]. These Pb islands protrude 0.5 nm or more from the first Pb layer, which corresponds to at least two additional Pb layers. An atomic resolution STM image at the area of a flat terrace clearly shows a close-packed lattice with a distance between the spots of ≈0.34 nm and a moiré pattern [Fig. 5(b)]. Therefore, the protrusions correspond to the overlayer Pb atoms

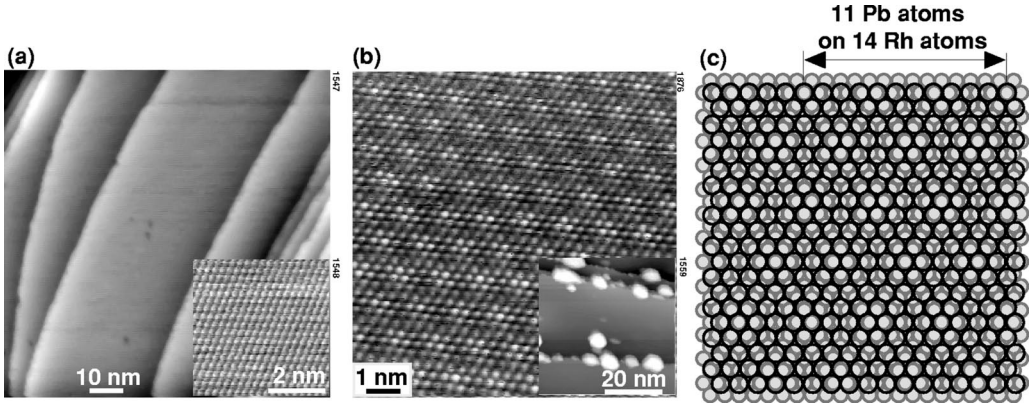

FIG. 5. (a) Large-scale STM image (100×100 nm^2) of Pb/Rh(111) at subsaturation coverage ($\theta_{Pb}=0.5$ ML, $V=-0.9$ mV, $I=1.1$ nA). The inset shows a high-resolution STM image (5×5 nm^2) at the same coverage ($V=-0.7$ mV, $I=4.5$ nA). (b) Atomically resolved STM image of the incommensurate Pb overlayer at oversaturation coverage (10×10 nm^2, $V=-0.5$ mV, $I=2.3$ nA). The inset shows a corresponding large-scale STM image ($\theta_{Pb}=1.0$ ML, 50×50 nm^2, $V=-60$ mV, $I=0.5$ nA). (c) Model of a Pb layer compressed by 2.2% with respect to bulk Pb on the Rh(111) substrate, resulting in a moiré structure.

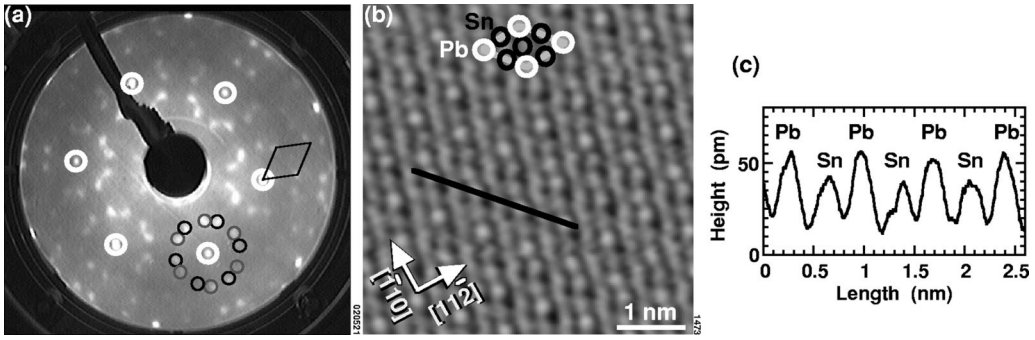

FIG. 6. (a) LEED pattern at 141 eV incident electron energy of the (Pb,Sn)/Rh(111) surface at a coverage of 0.16 ML Pb and 0.42 ML Sn. The first-order Rh(111) substrate spots are marked by thick white circles. Two different orientations ($\pm 19°$) of ($\sqrt{7}\times\sqrt{7}$) spots are marked by gray and black open circles. The reciprocal ($\sqrt{7}\times\sqrt{7}$) unit cell is illustrated by the black rhomb in (a). (b) Atomically resolved STM image of the ($\sqrt{7}\times\sqrt{7}$)-(Pb,Sn) phase (5×5 nm^2, $V=-0.4$ mV, $I=4.5$ nA). (c) Section profile along the black line in (b).

forming the incommensurate structure. A hard-sphere model for the Pb-Rh interface showing the moiré structure is displayed in Fig. 5(c). The Pb layer is compressed by 2.2% with respect to the Pb bulk lattice constant, resulting in a periodicity of roughly 11 Pb atoms on 14 Rh atoms. The nearest-neighbor distances are approximately 0.359 nm for (4×4)-Pb and 0.342 nm for IC-Pb, which are both very close to the atomic size (0.350 nm) of bulk Pb. This compression of the Pb layer with increasing coverage is similar to the Pb/Cu(111) system.[16]

C. Pb-Sn bimetallic films on Rh(111)

Various combinations of Pb-Sn films at coverages between 0.1 and 1.0 ML were examined by means of LEED, AES, and STM to identify whether Pb and Sn form an alloy or not. At a coverage of 0.17 ± 0.05 ML and 0.40 ± 0.05 ML for Pb and Sn, respectively, a new surface phase emerged, as shown below. This is the only 2D alloy phase we found for Pb-Sn films.

Figures 6(a) and 6(b) show a typical LEED pattern and an atomically resolved STM image of the bimetallic film at 0.16 ML and 0.42 ML for Pb and Sn, respectively. In this combination of the Pb and Sn coverage, a new LEED pattern identified as $(\sqrt{7}\times\sqrt{7})R\pm 19°$ appears, as shown in Fig. 6(a). Since neither pure-metal Pb nor Sn films on Rh(111) form a ($\sqrt{7}\times\sqrt{7}$) structure, it is concluded that this new structure is formed by a bimetallic Pb-Sn alloy film. There are two equivalent orientations marked by gray and black open circles around a first-order substrate spot in Fig. 6(a). An atomic-resolution STM image shows one bright protrusion and three darker protrusions in a ($\sqrt{7}\times\sqrt{7}$) unit cell, as shown in Fig. 6(b). Figure 6(c) shows a line section profile of the STM image in Fig. 6(b). The nearest-neighbor distance in a perfect ($\sqrt{7}\times\sqrt{7}$) structure of the kind observed here is 0.356 nm, close to the atomic distances of the (4×4)-Pb (0.359 nm) and $c(2\times4)$-Sn (0.356 nm) structures. Strictly speaking, this ($\sqrt{7}\times\sqrt{7}$) structure is an incommensurate phase, and we estimate from the LEED super-

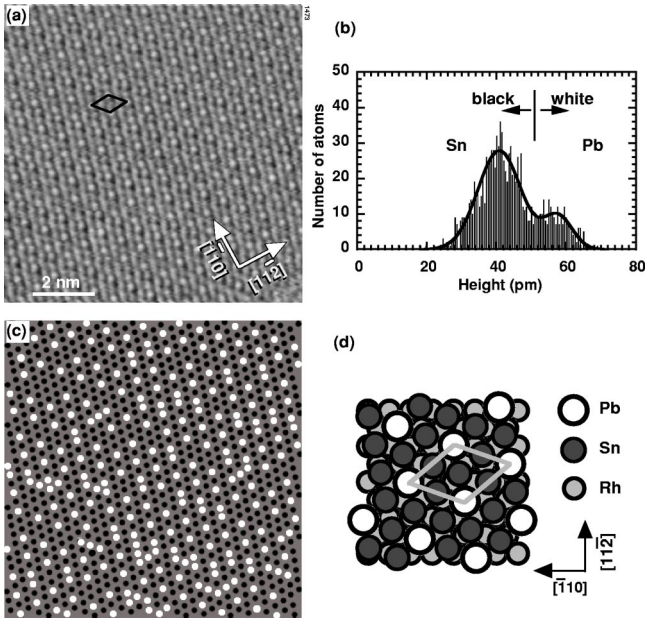

FIG. 7. (a) High resolution STM image of the ($\sqrt{7}\times\sqrt{7}$)-(Pb,Sn) phase (10×10 nm^2, $V=-0.4$ mV, $I=4.5$ nA). The unit cell of ($\sqrt{7}\times\sqrt{7}$) is illustrated by a black rhomb. (b) Histogram of apparent heights of the overlayer atoms. (c) Space distribution of two different apparent height values obtained from the STM image (a). (d) Structure model of the Rh(111)($\sqrt{7}\times\sqrt{7}$)-(Pb,Sn) surface.

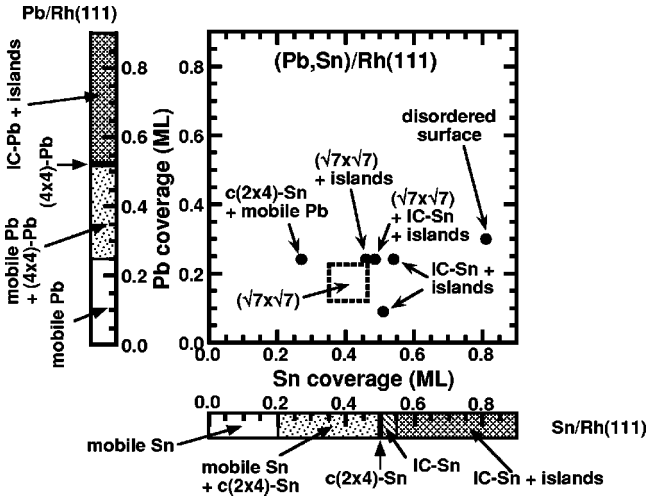

FIG. 8. A phase diagram of the (Pb,Sn)/Rh(111) system.

structure spots as well as from the STM images that the unit cell is expanded on average by approximately 5% with respect to a perfect $(\sqrt{7}\times\sqrt{7})$ structure. The expansion seems to be anisotropic in many places, as judged from the fine structure in the LEED spots as well as the STM images.

Figure 7 shows an STM image (a) and a histogram of the apparent heights of the overlayer atoms (b). Figure 7(b) clearly shows a bimodal distribution of the apparent atomic heights. By fitting sum of two Gaussians to the height distribution in Fig. 7(b), the percentage of atoms appearing bright and dark is found to be $22\%\pm3\%$ and $78\%\pm3\%$, respectively, close to the ratio of 24:76 expected from the amount of Pb and Sn deposited. An illustration of the space distribution of two different corrugations found in the height distribution is shown in Fig. 7(c). Since the $(\sqrt{7}\times\sqrt{7})$-(Pb,Sn) is an incommensurate phase and the contrast between brighter and darker protrusions depends on the tip quality, it is likely that the difference of apparent heights is not due to the different adsorption sites on the Rh(111) substrate. As shown by the line section profile in Fig. 6(c), the corrugation maximum for Pb is $\approx$20 pm higher than the corrugation maximum for Sn, which is a typical value for chemical contrast.[17,18] Since the atomic radii for Pb and Sn are 175 pm and 145 pm, respectively, the height difference of the spots may be related to the difference of the atomic radii of Pb and Sn. From these results, it is concluded that Pb and Sn atoms are imaged as brighter and darker protrusions, respectively. A structure model of the $(\sqrt{7}\times\sqrt{7})$-(Pb,Sn) structure is shown in Fig. 7(d).

Finally, Pb-Sn phases close to the nominal coverages of the $(\sqrt{7}\times\sqrt{7})$-(Pb,Sn) structure were examined. When the Sn coverage was higher or lower than nominal coverages of the $(\sqrt{7}\times\sqrt{7})$-(Pb,Sn) structure, the IC-Sn phase or domains of a $c(2\times4)$-Sn phase were formed, respectively. Then, Pb atoms did not mix with Sn and, at low coverage, were mobile on the surface. On the contrary, when the Pb coverage was higher or lower than the nominal coverage in the $(\sqrt{7}\times\sqrt{7})$-(Pb,Sn) structure, the $(\sqrt{7}\times\sqrt{7})$-(Pb,Sn) structure was formed in whole or part of the surface, respectively. Excess Pb or Sn atoms formed Pb islands or a $c(2\times4)$ phase, respectively. A phase diagram of (Pb,Sn)/Rh(111) system based on these data is shown in Fig. 8.

IV. DISCUSSION

The combined results of our LEED, STM, and AES measurements show the following similarities between the single metal films of Pb and Sn on the Rh(111) surface. At low coverage, both Pb and Sn atoms form islands on the Rh(111) surface at RT, but nevertheless are mobile enough to pose problems to imaging by STM. Although both Pb and Sn form bulk alloys with Rh, at room temperature neither Pb nor Sn form a surface alloy with the Rh substrate but they just form overlayer structures. We attribute this to the high stability of the Rh(111) surface. When all of the surface is covered with an overlayer, with increasing coverage and, hence, increasing chemical potential of Pb or Sn, the structures of these overlayers are compressed and change from commensurate phases into incommensurate phases whose atomic arrangements are closely related to the commensurate phases. As expected, due to the significantly smaller surface energies of Pb and Sn compared to that of Rh(111), both Pb and Sn films grow in Stranski-Krastanov mode. In both cases, islands start to form at the step edge. The height of the three-dimensional Pb islands is 0.5 nm or higher from the first Pb layer, which corresponds to at least two Pb layers, while the height of Sn islands is 0.3–0.5 nm from the first Sn layer, which correspond to one to two Sn layers. The height of the islands might be related to quantum-size effects.[19] The main difference between the Pb and Sn films is the symmetry of the atomic arrangement in the first monolayer. The Pb films form hexagonal close-packed structures that have sixfold symmetry, while Sn films form squarelike structures that have twofold symmetry. These results suggest that Sn atoms bind in-plane via the *sp* orbitals, leading to fourfold coordination with longer bond lengths in the surface as compared to bulk α-Sn. On the other hand, Pb atoms form metallic bonding with six nearest-neighbor atoms for both (4×4)-Pb and IC-Pb, resulting in close-packed structures similar to bulk Pb.

Among all bimetallic films of Pb-Sn on Rh(111) studied, we have found one composition where an ordered 2D alloy with a structure close to $(\sqrt{7}\times\sqrt{7})$ is formed. The formation of this 2D alloy is in sharp contrast to the immiscibility of Pb and Sn in the bulk. Since the 2D Pb-Sn alloy is actually incommensurate to the Rh(111) substrate, it cannot be considered a structure induced by the particular structure and/or lattice constant of the substrate. The Pb-Sn 2D alloy must be rather seen as a genuine property of the two-dimensional Pb-Sn system. In the bulk, Pb has a close-packed fcc structure and Sn forms a diamond lattice (α-Sn) or tetragonal (β-Sn) structures. Moreover, the 2D structures on Rh(111) are also different: Pb and Sn form structures with sixfold and fourfold coordination, respectively, which are the reminiscent of 3D structures. It is interesting to note that the ordered 2D alloy structure with a composition of roughly $PbSn_3$ assumes the lattice type of the minority element Pb, a close-packed lattice with sixfold coordination. The relatively large interatomic distances in the ordered 2D alloy (approximately 5% above that of the low-coverage structures of pure Sn or Pb) might be related to the unusually high sixfold in-plane coordination of Sn.

V. SUMMARY

The single and binary metal two-dimensional films of Pb and Sn on Rh(111) have been studied using STM, LEED, and AES at RT. Both Pb and Sn atoms are mobile at low coverage and form monolayer islands. With increasing coverage, the surface structures of both Pb and Sn change from commensurate phases into incommensurate phases. Both films grow in Stranski-Krastanov mode. There are many similarities between the Pb and Sn films on Rh(111) except the symmetry of atomic arrangement of the monolayer films. Pb films have a close-packed lattice with sixfold symmetry, while Sn films have twofold symmetry and fourfold in-plane coordination.

Bimetallic films of Pb and Sn on Rh(111) show an ordered 2D alloy with a structure close to $(\sqrt{7}\times\sqrt{7})$, although Pb and Sn are immiscible in the bulk. The Pb-Sn film has a close-packed structure and a composition of $PbSn_3$. This is, to our knowledge, the first observation of a 2D alloy of immiscible metals with a structure unrelated to the substrate. We consider it interesting to study other combinations of immiscible atoms, such as Pb-Cu, Ag-Cu, etc., to better understand the properties of 2D alloys.

ACKNOWLEDGMENTS

One of the authors (J.Y.) gratefully acknowledges financial support by the bilateral program for scientist exchange between Federal Ministry of Science and Transport of Austria and Japan Society for Promotion of Science (JSPS). This work was supported by the Austrian *Fonds zur Förderung der wissenschaftlichen Forschung* (START-program Y75).

*Corresponding author. Electronic address: j-yuhara@nucl.nagoya-u.ac.jp

[1] J. A. Rodriguez, Surf. Sci. Rep. **24**, 223 (1996).
[2] *The Chemical Physics of Solid Surfaces*, edited by D. A. King and D. P. Woodruff (Elsevier, Amsterdam, 1997), Vol. 8.
[3] L. Pleth Nielsen, F. Besenbacher, I. Stensgaard, E. Laegsgaard, C. Engdahl, P. Stoltze, K. W. Jacobsen, and J. K. Nørskov, Phys. Rev. Lett. **71**, 754 (1993).
[4] H. Röder, R. Schuster, H. Brune, and K. Kern, Phys. Rev. Lett. **71**, 2086 (1993).
[5] C. Nagl, O. Haller, E. Platzgummer, M. Schmid, and P. Varga, Surf. Sci. **321**, 237 (1994).
[6] C. Nagl, M. Pinczolits, M. Schmid, P. Varga, and I. K. Robinson, Phys. Rev. B **52**, 16 796 (1995).
[7] C. Nagl, E. Platzgummer, O. Haller, M. Schmid, and P. Varga, Surf. Sci. **331-333**, 831 (1995).
[8] D. Nakamura, J. Yuhara, and K. Morita, Appl. Surf. Sci. **130/132**, 72 (1998).
[9] J. Yuhara, D. Nakamura, K. Soda, and K. Morita, Surf. Sci. **482/485**, 1374 (2001).
[10] J. Yuhara, S. Yuasa, O. Yoshimoto, D. Nakamura, K. Soda, and M. Kamada, Nucl. Instrum. Methods Phys. Res. B **199**, 422 (2003).
[11] J. Yuhara, T. Takada, D. Nakamura, K. Soda, and M. Kamada, Mater. Sci. Eng., B **96**, 145 (2002).
[12] C. Mottet, G. Tréglia, and B. Legrand, Phys. Rev. B **46**, 16 018 (1992).
[13] S. M. Foiles, Surf. Sci. **292**, 5 (1993).
[14] C. Nagl, M. Schmid, and P. Varga, Surf. Sci. **369**, 159 (1996).
[15] H. Over and S. Schwegmann, Surf. Sci. **360**, 271 (1996) and references therein.
[16] G. Meyer, M. Michailov, and M. Henzler, Surf. Sci. **202**, 125 (1988).
[17] M. Schmid, H. Stadler, and P. Varga, Phys. Rev. Lett. **70**, 1441 (1993).
[18] M. Schmid and P. Varga, in *The Chemical Physics of Solid Surfaces*, edited by. D. P. Woodruff (Elsevier, Amsterdam, 2002), Vol. 10, Chap. 4, pp. 118–151.
[19] P. J. Feibelman and D. R. Hamann, Phys. Rev. B **29**, 6463 (1984).